Int J Adv Manuf Technol (2009) 40:316–323
DOI 10.1007/s00170-007-1327-y

ORIGINAL ARTICLE

Thermal modeling of the material removal rate and surface roughness for die-sinking EDM

K. Salonitis · A. Stournaras · P. Stavropoulos · G. Chryssolouris

Received: 3 May 2006 / Accepted: 19 November 2007 / Published online: 11 January 2008

Abstract The die-sinking electrical discharge machining (EDM) process is characterized by slow processing speeds. Research effort has been focused on optimizing the process parameters so as for the productivity of the process to be increased. In this paper a simple, thermal based model has been developed for the determination of the material removal rate and the average surface roughness achieved as a function of the process parameters. The model predicts that the increase of the discharge current, the arc voltage or the spark duration results in higher material removal rates and coarser workpiece surfaces. On the other hand the decrease of the idling time increases the material removal rate with the additional advantage of achieving slightly better surface roughness values. The model's predictions are compared with experimental results for verifying the approach and present good agreement with them.

Keywords EDM · Material removal rate · Surface roughness · Process modeling

Abbreviations

EDM	electrical discharge machining
FEA	finite element analysis
MRR	material removal rate
NOP	number of pulses
TWR	tool wear ratio

K. Salonitis · A. Stournaras · P. Stavropoulos · G. Chryssolouris (✉)
Laboratory for Manufacturing Systems and Automation, Department of Mechanical Engineering and Aeronautics, University of Patras, Patras 261 10, Greece
e-mail: gchrys@hol.gr

Nomenclature

A	Constant parameter depending on the workpiece material
a	Depth (μm)
a_w	Thermal diffusivity (m^2/sec)
B	Constant parameter depending on the workpiece material
c_p	Specific heat (J/kg.K)
d_c	Diameter of the crater (μm)
I	Discharge current (A)
k	Thermal conductivity (W/m.K)
L_v	Latent heat of vaporisation (kJ/kgr)
MRR	Material removal rate (mm^3/min)
NOP	Number of pulses (–)
p	Heat generated during the spark discharge (W)
q_w	Heat source intensity distribution (kW/mm^2)
R_a	Average surface roughness (μm)
R_{max}	Maximum surface roughness (μm)
R_w	Fraction the heat generated that enters the workpiece (–)
r_c	Radius of the crater (μm)
r_s	Heat input radius (μm)
s	Depth of crater (μm)
T	Temperature (°C)
T_s	Erosion front temperature (°C)
T_o	Ambient temperature (°C)
t	Time (s)
t_{mach}	Machining time (s)
t_i	Idling time ("off" time) (μs)
t_s	Spark duration ("on" time) (μs)
U_a	Arc voltage (Volt)
V_c	Volume removed per spark (mm^3)
ρ	Density (kgr/m^3)

1 Introduction

The electrical discharge machining (EDM) has gained importance due to its capability to remove material with good accuracy and precision. EDM accomplishes shapes that could hardly been achieved with any other conventional method, regardless the hardness of the material to be machined [1].

The main concern is the optimization of the process parameters for improving the output characteristics, i.e., maximize the material removal rate (MRR) and simultaneously minimize the tool wear rate (TWR) and the surface roughness (CLA value). A number of attempts to model the process have been reported in the literature by utilizing analytical, numerical or empirical methods.

The first theoretical models presented used one-dimension thermal models for the simulation of the process [2]. More elaborated theoretical approaches utilized two-dimensional heat transfer models [3–7]. In the most recent attempts, finite element analysis (FEA) is used for determining the temperature field induced within the workpiece due to EDM processing [7–10]. An alternative approach to model the material removal for a short pulsing duration was also introduced and took into consideration the electrostatic forces that act on the processed surface [11]. In most of the studies only the heating of the workpiece was considered. Few studies [11–13] have included modeling of the breakdown and plasma phases that lead to the generation of the heat source in the workpiece surface.

The surface roughness of the processed workpiece has been investigated in most studies with the use of experimental approaches and statistical analyses [14–16]. In few studies, pure theoretical approaches have been proposed, using FEA [10] or analytical methods [17].

In this paper, a simple theoretical model is proposed for the determination of the MRR and the surface roughness as a function of the main process parameters, i.e., the arc voltage, the current, the spark duration, the idling time, etc. The theoretical predictions are compared with the experimental results.

2 Analytical approach

In order to develop a model capable of predicting the material removal rate, the crater geometry that each spark discharge produces on the workpiece surface, has to be determined. For this reason, it is assumed that the distance from the workpiece surface that the temperature exceeds the melting point coincides with the crater depth, neglecting therefore the formation of a recast layer. The crater is assumed to have circular paraboloid geometry and its diameter on the surface is determined from empirical relations.

2.1 Temperature distribution within workpiece

The crater's depth is determined from the temperature distribution within the workpiece. For the simplification of the thermal analysis, the problem is considered as a one – dimension conduction problem. It is assumed that the heat is transferred to the workpiece only by conduction. Therefore, the heat balance at the erosion front can be expressed as:

$$q_w = \rho L_v \frac{\partial s}{\partial t} - k\left(\frac{dT}{dz}\right)_{z=0} \tag{1}$$

where q_w is the heat source intensity distribution, L_v is the latent heat of vaporization, k is the thermal conductivity, ρ is the density and T is the temperature.

The heat source intensity distribution is considered uniform and is determined from the equation:

$$q_w = \frac{R_w p}{\pi r_s^2} \tag{2}$$

where R_w is the fraction the heat generated entering the workpiece, p is the heat generated during the spark discharge, and r_s is the heat input radius. The heat generated during the spark discharge can be estimated from the equation:

$$p = I \cdot U_a \tag{3}$$

where I is the discharge current and U_a is the arc voltage.

The fraction of the generated heat entering the workpiece depends on the thermal properties of the workpiece and electrode material and the dielectric used. Therefore, theoretically, the steel workpiece absorbs less heat due to its lower thermal diffusivity than copper electrodes do. Earlier theoretical studies [5–7] have calculated that approximately 8% of the generated discharge heat is absorbed from the workpiece. Therefore, in the present study, R_w is considered equal to 0.08.

It is well documented that the heat source diameter is a function of the evolution of the discharge channel. The discharge channel is influenced by the dielectric and electrode material and is time dependent [2, 6, 18]. For the purpose of this work, and for deriving a closed form solution, an average diameter, called "equivalent heat input radius", of the heat source is assumed as a function of the duration of the spark and the current [19]:

$$r_s = 2040 \times I^{0.43} t_s^{0.44} \tag{4}$$

where r_s is the heat input radius (in μm) and t_s is the spark duration.

In order for the erosion front velocity ($\partial s/\partial t$) to be determined, the temperature gradient at the erosion front should be determined as well. The temperature distribution

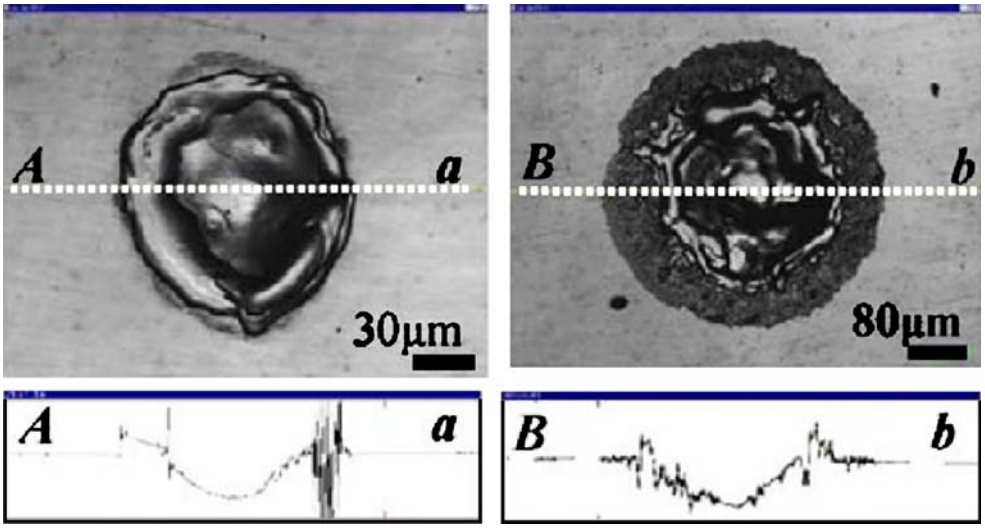

Fig. 1 Typical crater geometry and profile measured using confocal laser microscope scanner (**a**. Pulse duration equal to 10 μs and **b**. Pulse duration equal to 80 μs) [20]

inside the solid is governed by Fourier's partial differential equation of heat conduction into solids:

$$\frac{1}{a_w}\frac{\partial T}{\partial t} = \frac{\partial^2 T}{\partial z^2} \tag{5}$$

where a_w is the thermal diffusivity. The heat conduction equation can be rewritten as:

$$-\frac{1}{a_w}\left(\frac{\partial s}{\partial t}\right)\frac{dT}{dz} = \frac{d^2T}{dz^2} \tag{6}$$

The boundary conditions are:

$$T = T_s \text{ at } \quad z = 0 \tag{7}$$

$$T = T_0 \text{ at } \quad z \to \infty \tag{8}$$

By applying the boundary conditions, Eq. (6) can be solved for the temperature distribution inside the solid:

$$\frac{T - T_o}{T_s - T_o} = e^{-\frac{1}{a_w}\left(\frac{ds}{dt}\right)z} \tag{9}$$

The temperature gradient at the erosion front can be determined as:

$$\left(\frac{dT}{dz}\right)_{z=0} = -\frac{1}{a_w}\left(\frac{ds}{dt}\right)(T_s - T_o) \tag{10}$$

Substitution of the temperature gradient into the energy balance (Eq. 1) yields:

$$q_w = \rho L_v\left(\frac{ds}{dt}\right) + \rho c_p\left(\frac{ds}{dt}\right)(\mathrm{T}_s - \mathrm{T}_o) \tag{11}$$

where c_p is the specific heat.

Therefore, the velocity of the erosion front can be expressed as:

$$\frac{ds}{dt} = \frac{q_w}{\rho\left(L_v + c_p(\mathrm{T}_s - \mathrm{T}_o)\right)} \tag{12}$$

The depth s of the crater can be determined by integrating the previous equation:

$$s = \frac{q_w t_s}{\rho\left(L_v + c_p(T_s - T_o)\right)} \tag{13}$$

2.2 Crater geometry

Based on previous experimental results (Fig. 1), the crater formed due to spark discharge can be assumed to have circular paraboloid geometry (Fig. 2) that is described by the following equation:

$$\frac{x^2 + y^2}{r_c^2} = \frac{(s - z)}{s} \tag{14}$$

where r_c and s are the crater's radius and depth, respectively.

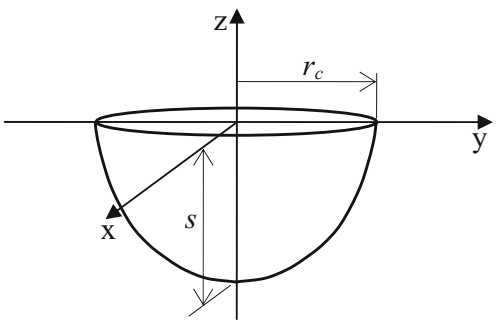

Fig. 2 Crater geometry

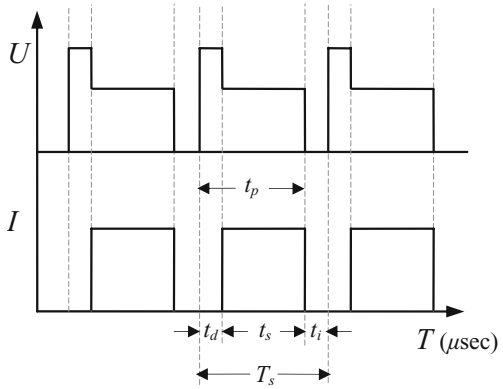

Fig. 3 Illustration of current and voltage variation over time

The crater's depth is determined from the melting isothermal (Eq. 13). Rebelo et al. [21] proved that a relation exists between the radius of the crater, the discharge current and the spark duration. The general form of this relation can be given by the following equation:

$$r_c = \frac{d_c}{2} = A \times (I \cdot t_s)^B \tag{15}$$

where r_c and d_c are the radius and the diameter of the crater respectively (in μm), I is the discharge current, t_s is the spark duration, and A and B are constants that depend on the workpiece material. For the present study, constants A and B are considered to be equal to the ones estimated by Rebelo et al. [21] for the case of martensitic steels used in the manufacturing of dies, i.e., A=2087/2 and B=0.37.

Therefore, the volume removed per spark V_c can be determined by equation:

$$V_c = \frac{1}{2}\pi s r_c^2 \tag{16}$$

2.3 Material removal rate (MRR)

For estimating the *MRR*, the number of pulses occurring in the unit of time should be determined. As shown in Fig. 3, each spark cycle, T_s, is composed of three discrete stages. During the first stage, the electro-magnetic field is created between the electrode and the workpiece by polarizing the dielectric fluid. Once the resistance of the dielectric fluid has been minimized, the spark occurs generating the current that vaporizes the workpiece material. The time spent for building the electromagnetic field is characterized as the ignition delay time, t_d, which is negligible compared to the duration of the spark discharge, t_s. Between each spark discharge, an idling time, t_i, occurs that allows the removal of the debris generated.

Therefore, the number of pulses (*NOP*) can be determined from the process characteristic times:

$$(NOP) = \frac{t_{mach}}{t_s + t_i} \tag{17}$$

where t_{mach} is the machining time, t_s is the discharge duration ("on" time) and t_i is the idling time.

Knowing the number of pulses and the crater's volume, one can determine the *MRR* by the following equation:

$$MRR = \frac{V_c \cdot (NOP)}{t_{mach}} \tag{18}$$

Table 1 Thermal properties and chemical composition of St–37

Thermal property	**Value**
Heat conductivity	48 W/m.K
Specific heat	475 J/kgr.K
Latent heat of vaporization	2750 kJ/kgr
Density	7879 kgr/m^3
Chemical composition	**(wt%)**
Fe	Balance
C	0.20
Mn	0.40
P	0.04
S	0.05

2.4 Surface roughness

The maximum surface roughness can be assumed as being equal to the depth of the crater formed during an individual spark discharge; however, this is not the case for the average surface roughness. The finished workpiece surface

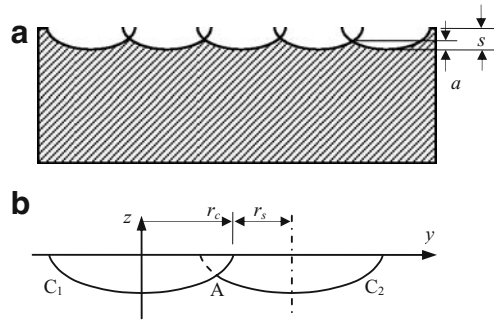

Fig. 4 Surface roughness

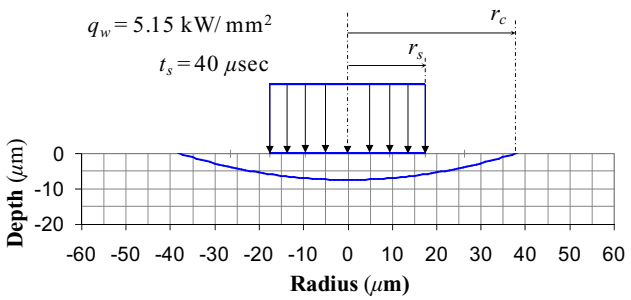

Fig. 5 Heat source equivalent radius and crater radius

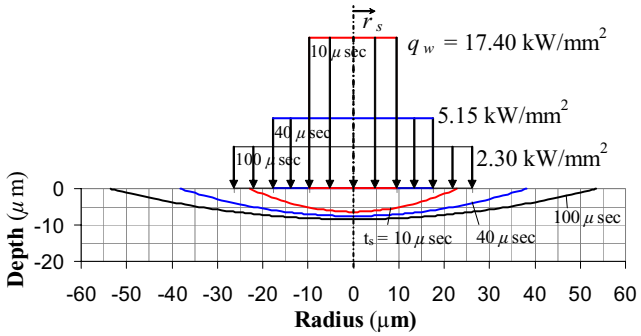

Fig. 6 Crater geometry and heat source for various spark durations

is the outcome of a series of overlapping craters as shown in Fig. 4a. It is therefore obvious that the maximum deviation of the workpiece surface will equal depth a, which thus defines the average surface roughness R_a. Zhang et al. [17] based on microscopic observations, approached depth a as being one third of the crater's depth.

The basic assumption for estimating the average surface roughness R_a is that besides the formed crater $C1$, another crater $C2$ can be formed on condition that the plasma can only be discharged on the surface of the workpiece and not on the flanks of the crater. Therefore, the axis of the heat source radius of the second crater ($C2$) will be in a distance equal to (r_c+r_s) from the axis of the first crater ($C1$) (Fig. 4b). Based on Eq. (14), the equations of both craters can be derived from:

$$\begin{aligned} &\mathrm{C1}: \frac{y^2}{r_c^2} = \frac{(s-z)}{s} \\ &\mathrm{C2}: \frac{(y-(r_c+r_s))^2}{r_c^2} = \frac{(s-z)}{s} \end{aligned} \tag{19}$$

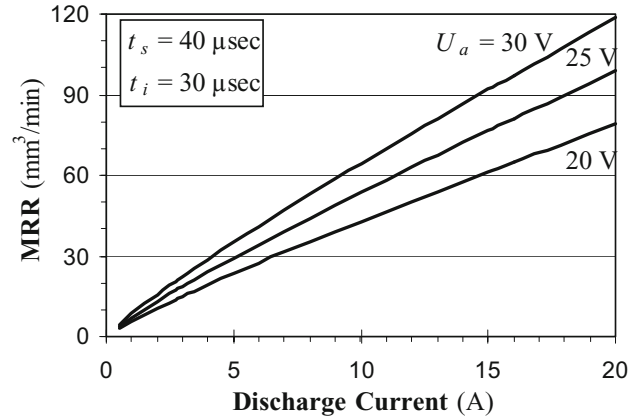

Fig. 7 Effect of discharge current and arc voltage on MRR

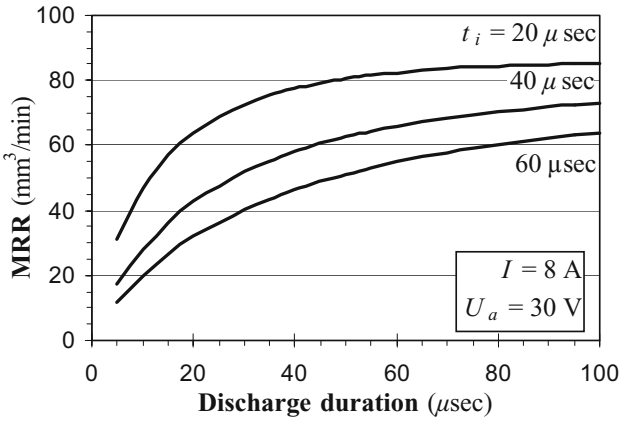

Fig. 8 Effect of discharge duration on MRR for various idling times

Setting parameters $y=y_A$ and $z=z_A$ in Eq. (19), the linear system can be solved for estimating depth a:

$$a = s - z_A = \frac{1}{4}\left[\frac{r_c + r_s}{r_c}\right]^2 s \tag{20}$$

Therefore the maximum surface roughness and the average surface roughness are given by Eqs. (21) and (22) respectively:

$$R_{\max} = s \tag{21}$$

$$R_a = \frac{1}{4}\left[\frac{r_c + r_s}{r_c}\right]^2 s \tag{22}$$

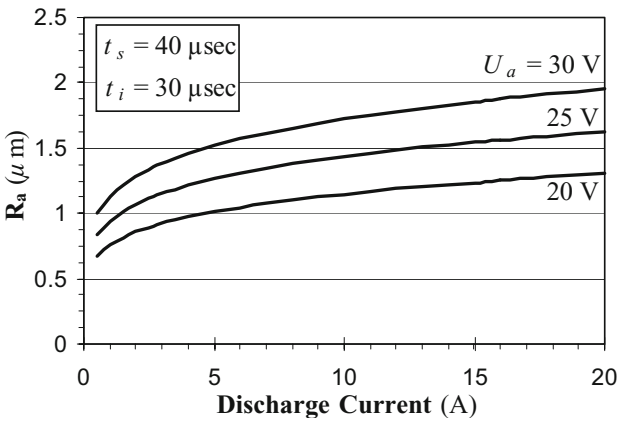

Fig. 9 Effect of discharge current and arc voltage on average surface roughness

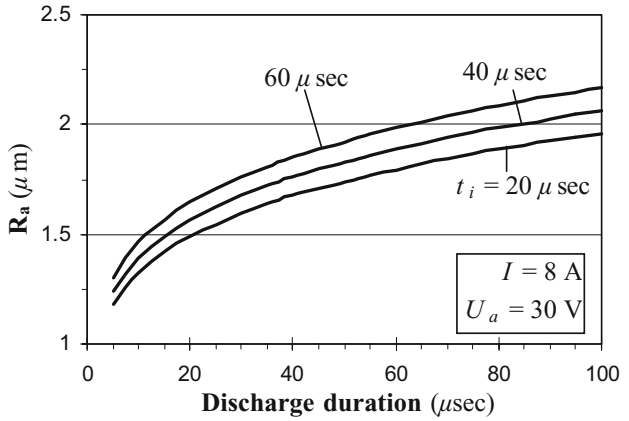

Fig. 10 Effect of discharge duration on average surface roughness for various idling times

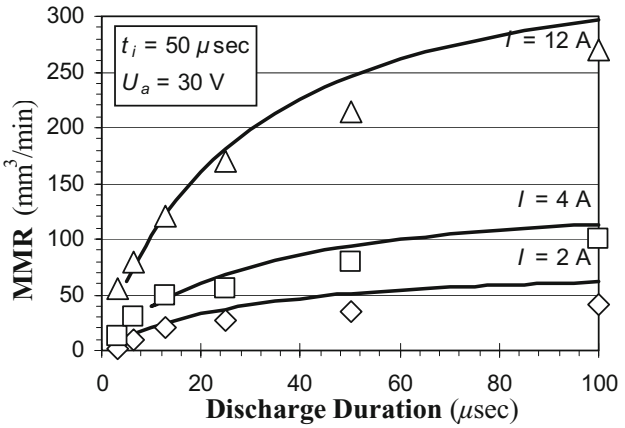

Fig. 11 Comparison between experimental results and theoretical predictions of MRR

3 Theoretical results and experimental verification

3.1 Theoretical results

The model developed was solved for the case of EDM processing of a steel (St–37) part with copper electrode. The thermal properties and the chemical composition of the workpiece material are presented in Table 1.

The crater depth and diameter were determined by Eqs. (13) and (15) respectively. Equation (14) describes the geometry of the crater formed. In Fig. 5 the heat source and the equivalent heat source radius are illustrated. It can be clearly seen that the heat source equivalent diameter is larger than the crater geometry. In Fig. 6, the crater geometry dependence on discharge duration is shown. The model predicts larger crater depths for increased sparking durations and agrees with the predictions presented by Schulze et al. [9].

Figure 7 shows that the model predicts the increase of the *MRR* with that of the discharge current and with the increase of the arc voltage. This prediction is justified by the fact that either the increase of the current or that of the arc voltage results in higher heat input rates entering the workpiece and thus, larger craters are formed.

Furthermore, the *MRR* increases with the increase of the spark duration as illustrated in Fig. 8. Increased discharge duration results in more energy entering into the workpiece per pulse, and consequently, more material is melted and removed forming a larger crater. In the same figure it can be seen that the increase of the idling time reduces the *MRR*, which is justifiable should it be considered that the increase of the idling time results in fewer discharges per unit of time. Among the various parameters involved in the process, it is indicated that the arc voltage has the greatest effect on the *MRR*; however a statistical analysis is required in order to certify this result.

The average surface roughness is determined by Eq. (22). The effect of the discharge current and of the arc voltage on the average surface roughness is depicted in Fig. 9. In Fig. 10, it is illustrated that the average surface roughness is increased with the discharge duration, whilst the idling time has a very mild effect. The doubling of the

Table 2 Experimental machining parameters

Machining parameter	***I*** (A)	t_s (μs)	t_i (μs)	U_a (V)
Value	2, 4, 12	3.2, 6.4, 12.8, 25, 50, 100	5	30

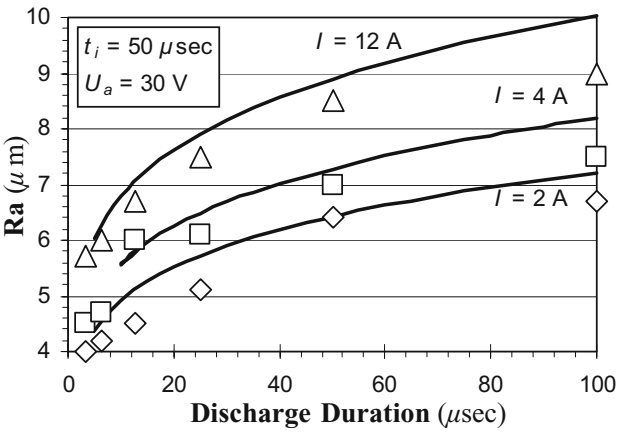

Fig. 12 Comparison between experimental results and theoretical predictions of average surface roughness

idling time results in an increase of the average surface roughness by less than 10%. This tendency is in agreement with other published experimental results [22]. Once more, it was concluded that the arc voltage had the greatest effect on the average surface roughness, whereas the idling time hardly had any.

3.2 Experimental setup

A number of experiments were conducted in order for the effect of the current and the discharge duration in the MRR and the average surface roughness to be studied. The EDM conditions are presented in Table 2. A die-sinking CNC EDM machine (Charmilles Roboform 22) that has the ability to supply electrical current of 0.5 – 64 A was used for this reason. Rectangular shaped electrodes (10 mm× 20 mm) machined from electrolytic copper were used on pre-ground St–37 specimens with kerosene as a dielectric fluid. In order to comply with the assumption of negligible delay ignition time, the "open" voltage (ionization voltage) was set at 200 V and the arc voltage at 30 V. The total machining time was set to 8 min.

Once the experiments were performed, the *MRR* and the average surface roughness were measured. For the calculation of the *MRR*, the depth of cut was determined by sectioning the processed workpiece and using an optical microscope for the measurement (with an accuracy of 0.001 mm). The surface roughness was measured with the use of a Mitutoyo SJ–401 surface measuring instrument that had a resolution of 0.000125 μm.

3.3 Comparison between theoretical predictions and experimental results

Figure 11 shows the comparison of the experimentally determined *MRR* and the theoretical predictions for altering discharge duration and current. As it can be seen the model slightly overestimates the *MRR* (average deviation 8.2%). This is justified should it be taken into consideration that the model ignores the formation of the recast layer which reduces the *MRR*. Furthermore, this overestimation may be accounted for neglecting the delay ignition time, which results in larger spark durations and thus, in more energy, entering into the workpiece for the estimation of isothermal melting.

Figure 12, presents the comparison between the measured average surface roughness and the theoretically predicted one from Eq. (22). The average deviation between these two is ca. 6.1%. It can be noticed that the deviation is increased as the surface discharge duration also increases. This could be accounted for neglecting the formation of recast layer, which is enhanced when it is being processed with larger peak current values.

4 Conclusions

A theoretical thermal model has been proposed for the simulation of the die-sinking EDM process. The MRR and average surface roughness can be determined with an average deviation of 8.2 % and 6.1 %, respectively. The deviations are attributed to the assumptions posed during the development of the model, i.e., the neglect of the recast layer's formation and the assumption that the idling time is insignificant compared with the discharge duration.

References

1. Chryssolouris G (2005) Manufacturing systems-Theory and practice. 2nd (ed.), Springer, Berlin
2. Erden A, Kaftanoglou B (1981) Thermo-mathematical modeling and optimization of energy pulse forms in electric discharge machining (EDM). Int J Mach Tool D R 21:11–22
3. Van Coppenolle B, Dauw DF (1995) On the Evolution of EDM Research Part 1: Modeling and Controlling the EDM Process. Proc ISEM XI Int Symp for Electro-Machining, pp 117–131
4. Tariq Jilani S, Pandley PC (1982) Analysis and modelling of EDM parameters. Precis Eng 4(4):215–221
5. DiBitonto DD, Eubank PT, Patel MR, Barrufet MA (1989) Theoretical models of the electrical discharge machining process. I A simple cathode erosion model. J Appl Phys 66(9):4095–4103
6. Patel MR, Barrufet MA, Eubank PT, DiBitonto DD (1989) Theoretical models of the electrical discharge machining process. II The anode erosion model. J Appl Phys 66(9):4104–4111
7. Yadav V, Jain VK, Dixit PM (2002) Thermal stresses due to electrical discharge machining. Int J Mach Tool Manuf 42:877–888
8. Das S, Klotz M, Klocke F (2003) EDM Simulation: finite element-based calculation of deformation, microstructure and residual stresses. J Mater Process Tech 142:434–451
9. Schulze H-P, Herms R, Juhr H, Schaetzing W, Wolenber G (2004) Comparison of measured and simulated crater morphology for EDM. J Mater Process Tech 149:316–322
10. Marafona J, Chousal JAG (2006) A finite element model of EDM based on the Joule effect. Int J Mach Tool Manuf 46:595–602
11. Singh A, Ghosh A (1999) A thermo-electric model of material removal during electric discharge machining. Int J Mach Tool Manuf 39:669–682
12. Dhanik S, Joshi SS (2005) Modeling of a single resistance capacitance pulse discharge in micro-electro discharge machining. J Manuf Sci E–T ASME 127:759–767
13. Albinski K, Musiol K, Miernikiewicz A, Labuz S, Malota M (1995) Plasma temperature in electro-discarge machining. Proc ISEM XI Int Symp for Electro-Machining, pp 143–152
14. Karthikeyan R, Narayanan RPL, Naagarazan RS (1999) Mathematical modelling for electric discharge machining of aluminium-silicon carbide particulate composites. J Mater Process Tech 87:59–63
15. Chen Y, Mahdavian SM (1999) Parametric study into erosion wear in a computer numerical controlled electro-discharge machining process. Wear 236:350–354
16. Puertas I, Luis CJ, Alvarez L (2004) Analysis of the influence of EDM parameters on surface quality, MRR and EW of WC-Co. J Mater Process Tech 153–154:1026–1032
17. Zhang QH, Du R, Zhang JH, Zhang QB (2006) An investigation of ultrasonic-assisted electrical discharge machining in gas. Int J Mach Tool Manuf, In press

18. Erden A (1983) Effect of materials on the mechanism of electric discharge machining (EDM). J Eng Mater-T ASME 108:247–251
19. Ikai T, Hashigushi K (1995) Heat input for crater formation in EDM. Proc ISEM XI Int Symp for Electro-Machining, pp 163–170
20. Tamura T, Kobayashi Y (2004) Measurement of impulsive forces and crater formation in impulse discharge. J Mater Process Tech 149:212–216
21. Rebelo JC, Dias AM, Mesquita R, Vassalo P, Santos M (2000) An experimental study on electro-discharge machining and polishing of high strength copper-beryllium alloys. J Mater Process Tech 103:389–397
22. Kiyak M, Cakýr O (2007) Examination of machining parameters on surface roughness in EDM of tool steel. J Mater Process Tech 191:141–144